EFFECT OF CALCINATION TEMPERATURE ON THE ADSORPTION PERFORMANCE OF MG/AL LAYERED DOUBLE HYDROXIDE NANOPARTICLES IN THE REMOVAL OF MEROPENEM ANTIBIOTICS

Yaseen Rashid Hasan* **Mohammed Ali A. Shaban**** **Mohammed A. Ibrahim****
Lect. **Lect.** **Prof.**
Mohanad J. M-Ridha*** **Haitham A. Hussein****
Prof. **Assist. Prof.**
Reconst. and Proj. Direct., Ministry of Higher Education and Scie. Research, Baghdad, Iraq*
Dep. of Civil Engineering, College of Engineering, Al-Nahrain University, Baghdad, Iraq**
Dep. of Environmental Engineering, College of Engineering, University of Baghdad, Iraq***
muhannadenviro@coeng.uobaghdad.edu.iq

ABSTRACT

Meropenem (MER) antibiotic is removed from an aqueous solution using Mg-Al-layered double hydroxide (Mg/Al-LDHs) which serves to functionalize the principal object of enquiry in this paper–sunflower husks (SFH). The former sample demonstrated a 51% removal of MER while the latter demonstrated a 67% removal of MER. One of the areas explored was the impact of the rise calcination temperatures resulted in a concurrent increase in the surface area and porosity of LDHs which, in turn, provoked a heightened removal efficacy of MER at calcination temperatures between 300 °C and 350 °C. Nonetheless, LDHs experienced structural deformation and thus, diminished removal efficacy of MER when the calcination temperature was over 350 °C. The ideal adsorption conditions were determined via the undertaking of multiple batch studies. Adsorption process was implemented successfully with removal efficiency of 98% under optimal conditions. The adsorption of MER was found to be regulated by the chemisorption mechanism of the best suited second order kinetic model. The adsorption process seemed to be heterogeneous and on a multi-layer as suggested by the high determination coefficient with Freundlich model. Enhanced functional and structural properties were witnessed in this novel adsorbent's adsorption capacity, thereby highlighting its proficiency as an alternative.

Keywords: Meropenem, Adsorption, Sunflower husks, Layered double hydroxides, Calcination Temperature.

تأثير درجة حرارة التكلس على اداء الامتزاز لجزيئات هيدروكسيد النانوية مزدوجة الطبقات المغنسيوم / الالمنيوم في ازالة المضادات الحيوية الميروبينيم

ياسين رشيد حسن محمدعلي اكرم شعبان محمد عبد الخالق إبراهيم مهند جاسم محمدرضا هيثم علاء حسين
مدرس مدرس أستاذ أستاذ أستاذ مساعد
وزارة التعليم العالي جامعة النهرين جامعة النهرين جامعة بغداد جامعة النهرين
والبحث العلمي كلية الهندسة كلية الهندسة كلية الهندسة كلية الهندسة
مديرية الاعمار قسم الهندسة المدنية قسم الهندسة المدنية قسم هندسة البيئة قسم الهندسة المدنية والمشاريع

المستخلص

لإزالة المضادات الحيوية ميروبينيم من محلول المائي تم استخدام قشور عباد الشمس كمادة مازة مع هيدروكسيد مزدوج الطبقات من نوع Mg/Al–LDHs. تم اختبار قشور عباد الشمس قبل وبعدة اضافة Mg/Al–LDHs وتم الحصول على كفاءة ازالة 51٪ للميروبينيم قبل الاضافة Mg/Al–LDHsلقشور عباد الشمس في حين تم الحصول على كفاءة ازالة 67٪ للميروبينيم بعدة اضافة Mg/Al–LDHs لقشور عباد الشمس. وتم دراسة تأثير ارتفاع درجة حرارة التكلس إلى زيادة متزامنة في مساحة السطح ومسامية LDHs مما أدى بدوره إلى زيادة فعالية إزالة ميروبينيم في درجات حرارة التكلس بين 300 درجة مئوية و 350 درجة مئوية. ومع ذلك، شهدت LDHs تشوه الهيكلية، وبالتالي انخفاض فعالية إزالة ميروبينيم عندما كانت درجة حرارة التكلس أكثر من 350 درجة مئوية. تم تحديد ظروف الامتزاز المثالية من خلال إجراء دراسات متعددة. تم تنفيذ عملية الامتزاز بنجاح مع كفاءة إزالة 98٪ في ظل الظروف المثلى. وأظهرت نتائج الدراسة الحركية التي تم الحصول عليها ان النموذج الحركي من الدرجة الثانية واقترح ان الية الكيميائية تسيطر على الامتزاز ميروبينيم. واظهرت النتائج أن Freundlich هو النموذج الأنسب لوصف هذه العملية مع معامل ارتباط عالية، مما يشير إلى أن عملية الامتزاز كان على طبقة متعددة وغير متجانسة. هذه المواد المازة الجديدة هي بديل ممتاز لإزالة المضادات الحيوية من المحاليل المائية، وتحسين قدرة الامتزاز مع خصائص هيكلية ووظيفية أفضل.

الكلمات المفتاحية: ميروبينيم، الامتزاز، قشور عباد الشمس، هيدروكسيد مزدوج الطبقات، درجة حرارة التكلس.

Received:14/10/2021, Accepted:5/1/2022

INTRODUCTION

A significant public health and environmental issue has developed due the residuals and aggregation of the waste materials stemming from pharmaceutical compounds that see prevalent consumption within veterinary, medicine, and other such areas due to their notable benefits (17, 38, 45). Drinking water, ground water, surface water, and sewage discharge have all had traces of antibiotics and other pharmaceuticals identified within them (2,40). Livestock and human excretion, hospital wastewater, pharmaceutical effluent, and other such sources lead to the pollution of aquatic environments by pharmaceuticals (1, 37). Bacteria can form resistance to antibiotics following changes to microbial communities that stem from antibiotics being present in the environment (20, 57). Consequently, drinking water or the food chain can be compromised leading to humans absorbing the possibly toxic wastage that passes through aquatic organisms (30). Given that the health impacts of chronic and lifelong exposure to water with low doses of antibiotics are undetermined, the possible existence of low levels of antibiotics in drinking water is a significant worry to address (11). Thus, prior to the release of antibiotic wastewater into the environment, the antibiotics need to be eliminated or degraded. Pneumonia and meningitis are among the ample range of infections treated by the injectable β-lactam antibiotics meropenem (MER) which is part of the carbapenem group. The detection of a high ecological concentration of MER between µg/L and ng/L is possible as a result of its recurrent use (13, 56). The frequent use of MER for livestock and humans stems from its efficacy and quality as an antimicrobial (47). Upon one or more sensitive bacteria being present in severe infections or even before the diagnosis of the cause of an illness as an observational treatment, MER is often used (31). It has become one of the antibiotics most prevalently administers globally due to its effectiveness. However, the largest segment of MER is not metabolized and is consequently released into the environment, upon administration, despite its partial metabolization by enzymes and absorption by the gut (61). It is vital to remove MER from wastewater before it is discharged into the environment as there are already multiple Gram-negative and Gram-positive bacteria that were determined to be MER resistant (51). Diverse water sources have undergone multiple techniques to expunge the presence of antibiotics in the last decade or so. These include advanced oxidation processes (48), ozonation (9), electrocoagulation process (37, 38), extraction (8), Photo-Degradation by UV and UV/TiO2 Processes (43), nanofiltration membranes (25), chlorination (2), and Adsorption are among the mentioned techniques (23). The existence of multiple rate-controllable parameters, high removal efficacy, suitability for application over a large concentration range of sorbate, and low instrumentation cost are among the significant benefits of the adsorption process, making it one of the most efficient methods (11). Contaminated solutions have their adsorbates – pollutant molecules – diminished via the introduction of biosorbents, adsorbents, or sorbents, which are synthesized and natural materials in the mentioned treatment technique (36). Eliminating pollutants from wastewater through the adsorption process is one of the most efficacious techniques available. Furthermore, in cases where adsorbent availability is high and cost is low, employing this alternative treatment is an appealing prospect (53). Adsorbents that consist of agricultural waste, in its altered or initial form, have been the subject of much investigation by scientists in recent years (39). Expunging toxic pollutants from aqueous solutions can be effectively carried out via the incorporation of prevalently available and low-cost materials such as sunflower husks (SFH) (3), coke, wood, coal, and peat (5). Moreover, in the adsorption systems, multiple inorganic and organic matters are effectively removed by such materials (24). Chemical or physical alteration processes are often employed upon the vast majority of agricultural wastes, where such waste typically undergoes some kind of pre-treatment. The consequent adsorbent materials have their surface properties strengthened by such modification processes (41). Among the most vital of oil crops is the Helianthus annus, otherwise known as the sunflower. Biological waste material is left behind as a by-product in the form of the husk left by the sunflower seeds after industrial processing (46). Given that the fat and oil industry produce SFH as a waste product upon sunflower seed processing, SFH

was selected as an adsorbent (42, 49). Regarding water treatment, one kind of adsorbent that has demonstrated the most potential is nanomaterial-based adsorbents in recent years. The recyclability, improved stability, wider surface area, and non-toxicity of layered double hydroxides (LDHs)-containing hybrids make them the best performers with regard to adsorption and thus, an ideal material for water purification processes (15). LDHs are a class of layered anionic clay-composite that are used as part of a practical technique to alter the SFH biomass (61). Catalyst supports, anion exchangers, adsorbents, and catalysts are among the uses of LDHs that also boast an uncomplicated preparation process and resultantly, are considered be a material with great technological potential (10, 12, 54, 59). Non-framework interlayer anions react with the positively charged and main lamellar within the LDHs' non-covalent bond structure. The adsorption of distinct pollutants precedes a distinctive layered structure with other features including an elevated surface area and a high dispersion of cations and anions within LDHs (57). Due to the high adsorption ability and simple manufacturing process, LDHs have been the focal point of many academic works. Its use as an ion-exchange material or simple separation material is also possible and as previously mentioned, absorbers, catalyst supports, catalyst materials, and sorbents are other suitable uses for LDHs (31). The cutting-edge method for the preparation of LDHs is the slow pyrolysis of biomass waste, despite the multiple distinct methods available. The generation of products with stationary carbon skeletons is enabled via this new technology (57). Meanwhile, optimal cost and time taken figures are demonstrated when converting LDHs into several kinds of metal oxides upon burning the former at temperatures between 300 °C and 550 °C during the pyrolysis method (18). Resultantly, the LDHs pre-coated biomass reaction with the one-pot slow pyrolysis reaction can lead to the attainment of high-quality biomass supported LDHs. The production of double hydroxide materials such as SFH-Mg/Al-LDHs compounds that are toxic-free, readily divided, and innovative is a vital step in the effective use of LDHs to eliminate antibiotics from aqueous solutions. Meropenem (MER) antibiotic is removed from an aqueous solution using Mg-Al-layered double hydroxide (Mg/Al-LDHs) which serves to functionalize the principal object of enquiry in this paper – sunflower husks (SFH).

MATERIALS AND METHODS

Chemicals: London-based AstraZeneca enabled the attainment of MER. The physicochemical properties of MER are demonstrated by the following: chemical structure, as seen in Figure 1; molecular weight – 383.15g mol^{-1}; pKa – 6.624, 13.545, 2.661; and chemical formula – $C_{17}H_{25}N_3O_5S$. Sodium hydroxide (NaOH), hydrochloric acid (HCl), sodium carbonate (Na_2CO_3), and other sodium reagents were attained alongside magnesium nitrate hexahydrate ($Mg(NO_3)_2{\cdot}6H_2O$) and aluminum chloride hexahydrate ($AlCl_3{\cdot}6H_2O$) from Germany-based Merck – the commercial supplier and original manufacturer. This paper frequently utilized Merck Millipore Co.'s and Milli Q plus deionized water produced by the Millipore Mill-Q system. A resistivity above 18 MΩ cm was found within the water utilized in every experiment.

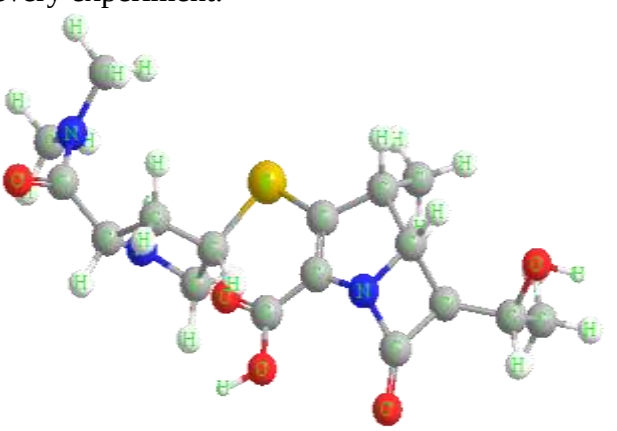

Fig. 1. Meropenem chemical structure (31)

Sunflower husk preparation

The dehusking of the sunflower seeds took place after they were bought from a local market. The surface adhered particles were removed by washing the SFH with distilled water multiple times. An oven at 80 °C is then used for precisely 1 day to dry the washed materials. This paper selected particle ranges 200 - 250 µm in size after the milling and sieving of dried materials. Future usage was enabled by using plastic bottles to store the specimens.

Synthesis of adsorbents

A temperature of 35 ± 2°C was implemented for the co-precipitation of the synthesized Mg/Al-LDHs. The M^{2+}/M^{3+} mole ratio was between 0.2 and 2 among the multiple Mg/Al

ratios utilized. A combination of two solutions makes up the technique. Contenting the wanted SFH dosage of 0.05, 0.1, 0.2, 0.5, 1, 1.5, and 2 g/50 mL occurs following the deionized water being used to dissolve the $Al(NO_3)_3.6H_2O$ (10.32 g) with $Mg(NO_3)_2.6H_2O$ (19.44 g) while mixing for 180 minutes at 120 rpm (Isolab, Germany) to produce the first solution. Subsequently, Whatman No.42 filter paper was used to filter each product. The second solution was produced by using deionized water to dissolve 1.4 g Na_2CO_3 and 9.2g NaOH and SFH from the first solution was incorporated into the second. A mixing rate of 5 mL/min was used for the first solution while stirring the second solution non-stop. Then, a stable pH value of 7 was guaranteed via the use of a pH measurement device (WTW 720, Germany) while half an hour of stirring was carried out upon the novel solution. Separation was performed via filter paper while a one-day period at a temperature of 115 °C occurred to develop the precipitates. Subsequently, NO_3^- was removed from the precipitates by washing them with deionized water. The SFH-Mg/Al-LDHs were generated by 10 hours of 105 °C to dry the wet solid. The adsorbents were calcined at distinct temperatures following the calcinations at 300 °C, 350 °C, and 400°C of the SFH-Mg/Al-LDHs.

Adsorption experiments

A batch mode was used to carry out the adsorption experiments. The dilution of the stock solution of MER – prepared by using 0.5 L of deionized water to dissolve 0.5 g – enabled the obtention of the 10–350 mg/l concentration of MER utilized in this paper. Under a temperature condition of -20 °C, a dark glass container was used to store the MER solution. 0.1M NaOH or 0.1M HCl were used to alter the pH of the working solutions to the wanted values. The Lovibond pH meter (Germany) was used to carry out the pH measurements. The adsorbent at distinct doses between 0.05 and 5 g/50 mL were combined with distinct pH between 2 and 9 and distinct initial concentrations between 10 and 350 mg/l of the 50 ml specimens of MER solutions. Distinct contact times between 3 and 360 minutes at room temperature were subjected to the mixtures situated on a shaker (LSI-3016R; Labtech, Korea) at 150 rpm after being placed within 250 ml Erlenmeyer flasks. A UV0Vis spectrophotometer (Shimadzu UV–1800, Japan) was used to analyze, at a maximum wavelength of 296 nm, the concentrations of MER in the filtrate, while a 0.45 µm pore-sized membrane (Whatman, Germany) was used to filter the specimens at the necessary contact time. The equation below was used to calculate the removal effectiveness (R%) of MER (14, 32):

$$R(\%) = \frac{(C_o - C_e)}{C_o} \times 100 \qquad (1)$$

The equilibrium and initial concentrations of the MER solution are represented by C_e and C_o (mg L^{-1}) respectively.

The variance in concentration between the resultant and initial adsorption was used to calculate the equilibrium adsorption capacity of MER (q_e, mg g^{-1}) via the equation below (23):

$$q_e = \frac{V(C_o - C_t)}{m} \qquad (2)$$

The concentration of MER at any time is represented by Ct (mg L^{-1}), while m represents the mass of the adsorbent (g) and V represents the volume of the solution (L).

RESULTS AND DISCUSSION

Adsorbents characterizations

X-ray diffraction pattern (XRD): Figure 2 portrays the x-ray diffraction patterns for layered double hydroxides biomass. Between 23° - 45° 2θ, the diffraction took place. Distinct calcination temperatures loaded XRD tests revealed clear variance between the findings of the raw SFH-MG/Al-LDHs and the SFH. Consequently, the separation process seems to be mechanically regulated by the chemical adsorption, given that the SFH-Mg/Al-LDHs experienced an alteration to its chemical composition (31).

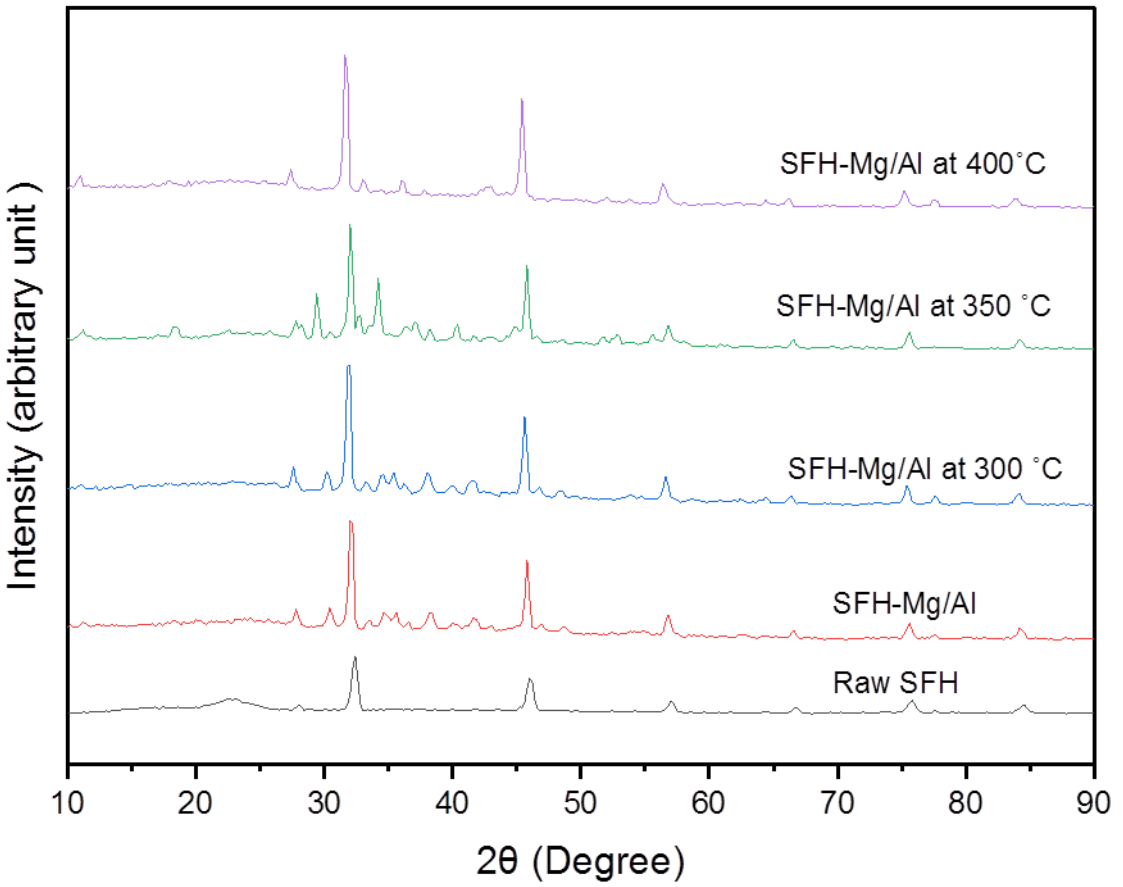

Fig. 2. XRD pattern of raw SFH-Mg/Al-LDHs at 300°C, SFH-Mg/Al-LDHs at 350°C, SFH-Mg/Al-LDHs at 400°C, SFH-Mg/Al-LDHs, and SFH adsorbents

Morphology

Figure 3 demonstrates how Scanning Electron Microscopy (SEM) was used to investigate the morphology of the raw SFH-Mg/Al-LDHs at 300°C, SFH-Mg/Al-LDHs at 350°C, SFH-Mg/Al-LDHs at 400°C, SFH-Mg/Al-LDHs, and SFH adsorbents. Figure 3b illustrates that synthesis of SFH with MG/Al-LDHs causes a total alteration to the morphological features of SFH, as seen in Figure 3a. Multiple divided and non-uniform aggregates as well as a rough surface characterize said adsorbent, as per the SEM of the SFH-Mg/Al-LDHs. Moreover, the outer wall of the SFH-Mg/Al-LDHs consists of elongated grooves and large chasms. This results in active sites for the sorbing of the adsorbate molecules as well as a high surface area, thereby demonstrating the benefit of such morphological features of the surface of the SFH-Mg/Al-LDHs. Upon the calcination temperature of 300 °C being reached, a substantial change in the morphological properties of the SFH-Mg/Al-LDHs occurs, as demonstrated by the SEM image of the SFH-Mg/Al-LDHs after being subjected to said temperature and made evident by comparing Figure 3b and 3c. The merging of multiple pre-separated aggregates is observed while a smoother surface also appears in the SFH-Mg/Al-LDHs. Nonetheless, many large ravines and grooves appear in the exterior biomass surface upon the calcination temperature reaching 350 °C, as seen in Figure 3d. Adsorbate molecules are captured more effectively due to the large surface area generated by such biomass morphological surface features. Miniscule pores and holes are observed in an irregular biomass morphology when a calcination temperature 400 °C is applied, as seen in Figure 3e. Figure 4 and Table 1 demonstrates the presence of Fe, Ca, K, C, K, O, Cl, P, Mg, Na, and Al which were detected at the distinct calcination temperatures following and prior to synthesis with Mg/Al-LDHs via the Energy Dispersive Spectrum (EDS) of biomass.

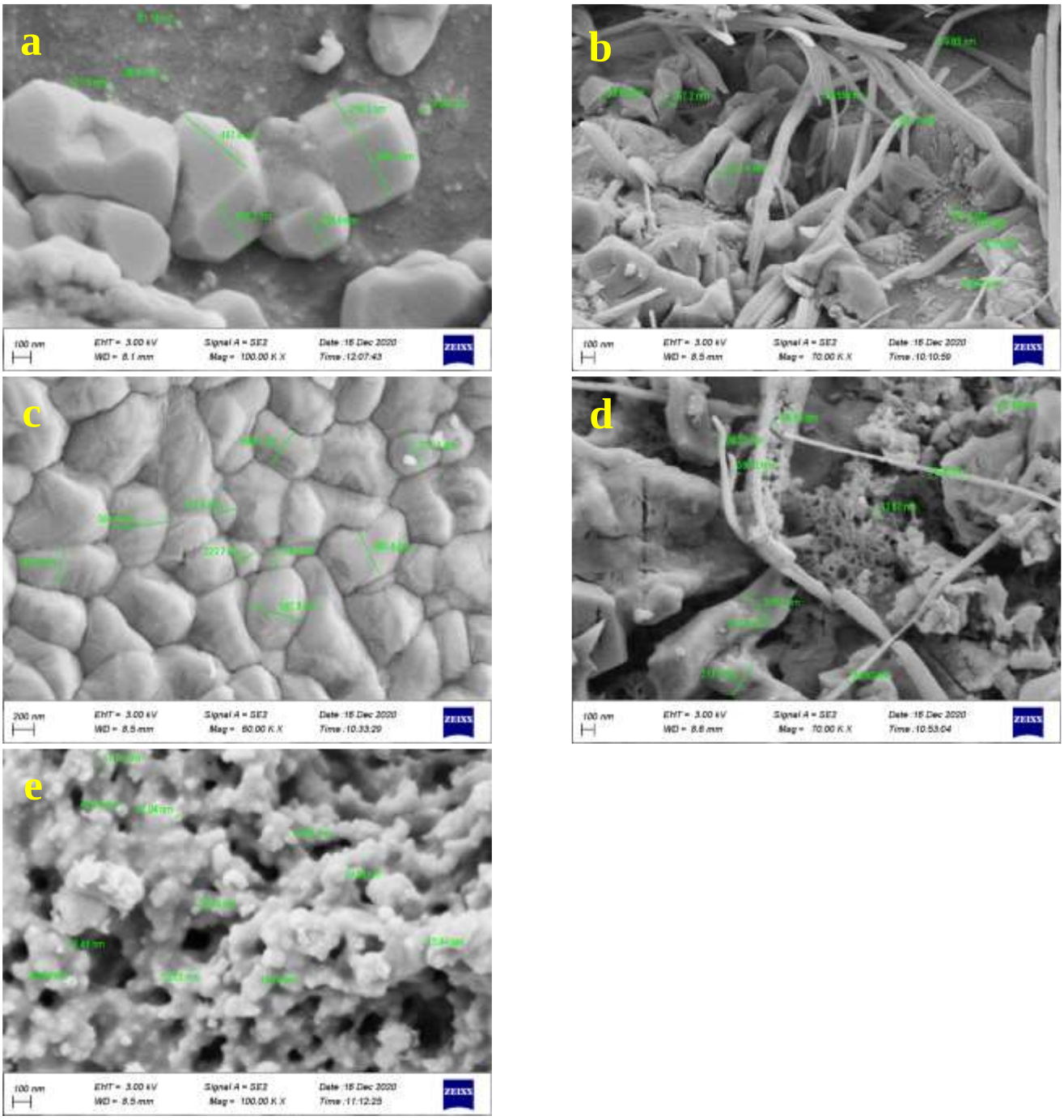

Fig. 3. SEM micrographs of (a) raw SFH, (b) SFH-Mg/Al-LDHs, (c) SFH-Mg/Al-LDHs at 300°C, (d) SFH-Mg/Al-LDHs at 350°C, and (e) SFH-Mg/Al-LDHs at 400°C adsorbents

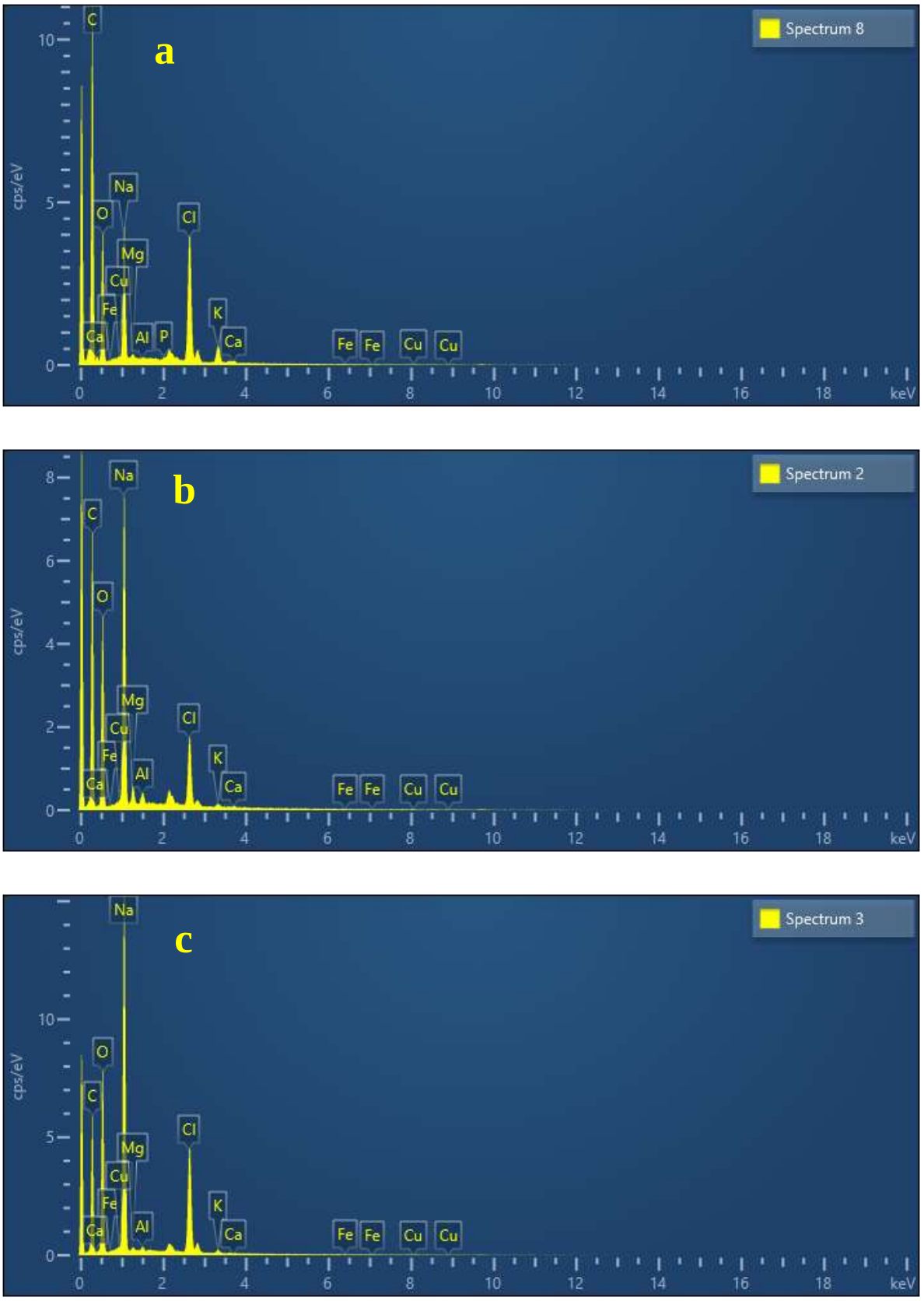
a
Spectrum 8
cps/eV
keV
C
Na
O
Cl
Mg
Cu
Fe
K
Ca
Al
P
Fe Fe Cu Cu
b
Spectrum 2
c
Spectrum 3

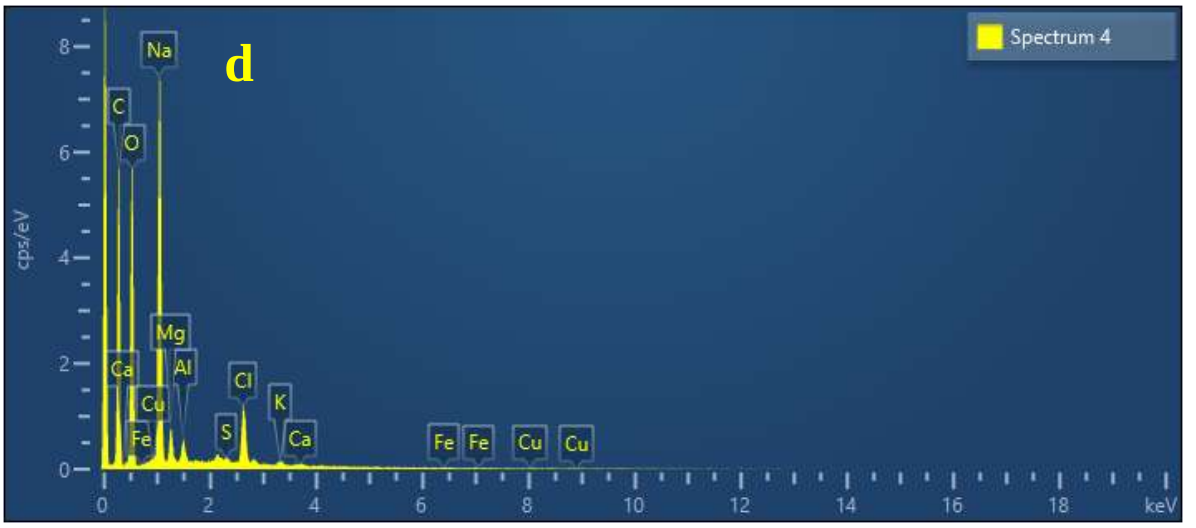

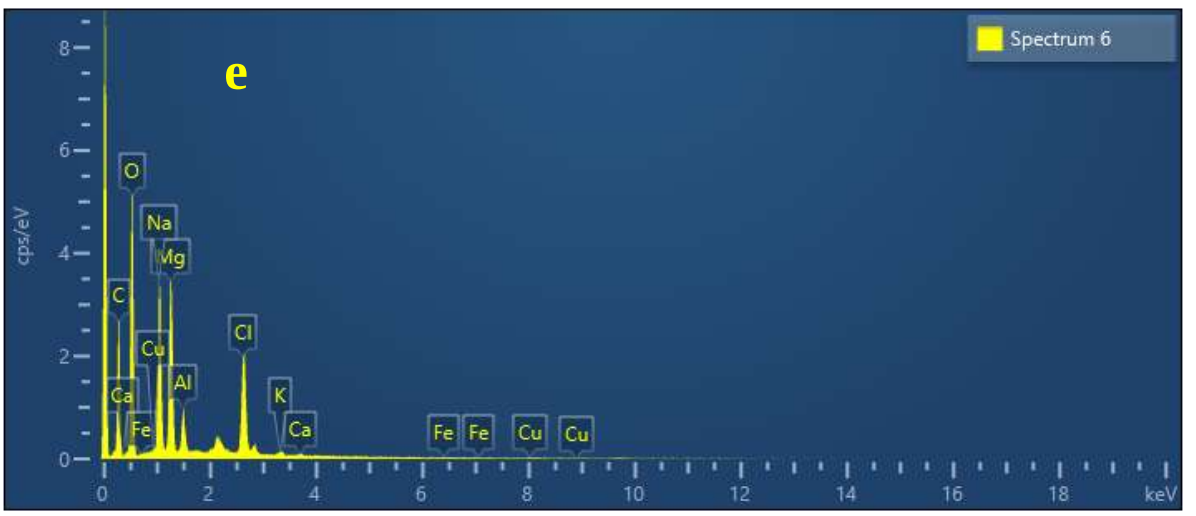

Fig. 4. EDS spectra of (a) raw SFH, (b) SFH-Mg/Al-LDHs, (c) SFH-Mg/Al-LDHs at 300°C, (d) SFH-Mg/Al-LDHs at 350°C, and (e) SFH-Mg/Al-LDHs at 400°C adsorbents

Table 1. elements percent of raw SFH, SFH-Mg/Al-LDHs, SFH-Mg/Al-LDHs at 300°C, SFH-Mg/Al-LDHs at 350°C, and SFH-Mg/Al-LDHs at 400°C adsorbents

raw SFH		SFH-Mg/Al-LDHs		SFH-Mg/Al-LDHs at 300°C		SFH-Mg/Al-LDHs at 350°C		SFH-Mg/Al-LDHs at 400°C	
Element	Weight %	Element	Weight %	Element	Weight %	Element	Weight %	Element	Weight %
C	66.54	C	55.98	C	46.87	C	50.40	C	42.39
O	22.49	O	28.60	O	31.12	O	33.78	O	37.51
Na	4.39	Na	10.97	Na	15.60	Na	11.59	Na	7.09
Cl	5.06	Cl	2.96	Cl	5.57	Cl	2.05	Mg	6.02
K	0.91	Mg	0.55	K	0.23	Mg	0.86	Cl	4.94
Ca	0.13	Al	0.33	Al	0.16	Al	0.51	Al	1.36
Fe	0.00	K	0.19	Fe	0.00	Ca	0.07	Ca	0.14
Cu	0.29	Ca	0.07	Cu	0.32	Fe	0.00	Cu	0.27
Al	0.02	Cu	0.30	Mg	0.12	Cu	0.36	Fe	0.04
P	0.06	Fe	0.05	Ca	0.02	K	0.18	K	0.24
Mg	0.09	Total	100.00	Total	100.00	S	0.18	Total	100.00
Total	100.00					Total	100.00		

Biosorbent preparation: he separation of MER from aqueous solutions within raw SFH-Mg/Al-LDHs and SFH biosorbent specimens was tested. The establishment of equilibrium was determined by stirring each solution for 4 hours following the addition 0.5 g of each biosorbent to 50 mL of 50 mg/L MER solution. The raw SFH-Mg/Al-LDHs sample demonstrated a 67% removal of MER while the raw SFH specimen demonstrated a 51% removal of MER, as per the findings of this paper. Thus, removal efficacy of MER was found to be greater when Mg/Al-LDHs were incorporated with the SFH. Eight hours of

distinct calcination temperatures between 300 °C and 400 °C was enacted upon the SFH-Mg/Al-LDHs specimen to investigate how MER separation is impacted by calcination temperatures. 0.5 g of calcined samples was added to 50 mL of 50 mg/L MER solution at 4 hours and percentage removal of MER was studied. Table 2 portrays the findings of said analysis where a decrease in the MER removal percentage was observed at temperatures beyond 350 °C, while up to said temperature, an increase was observed. At a calcination temperature of 350 °C, the SFH-Mg/Al-LDHs sample exhibited the maximum removal percentage, reaching 91%. As mentioned, a rise in removal percentage was witness when calcination temperatures rose up to 350 °C, which could be attributed to the concurrent increase in LDHs surface area and porosity as a result of higher temperatures. However, the reduction in the removal percentage could be attributed to LDHs structural deformations upon the calcination temperature superseding 350 °C (21).

Table 2. Impact of calcination temperature on removal percentage of MER

Biosorbents	Calcination temperature (°C)	Percentage removal of MER from 50 mg/L solution (%)
SFH-Mg/Al-LDHs	25	67
SFH-Mg/Al-LDHs	300	72
SFH-Mg/Al-LDHs	350	91
SFH-Mg/Al-LDHs	400	82

Impact of adsorbent dose

In the study of adsorption processes, one of the vital aspects is identifying the optimal adsorbent dose, particularly regarding the economic angle. The adsorbent dosage was enhanced via distinct quantities of biomass being used in the batch equilibrium experiments undertaken. Figure 5 illustrates the 4-hour contact time, 6 solution pH, and the MER removal efficacy dependence on the adsorbent dosage between 0.05 and 2 g/50 mL for the specimen of 100 mg/l initial concentration. Upon the biomass dosage rising from 0.05 to 1.50 g/50 mL, the removal efficacy of MER rose from 08% to 64% for raw SFH, 10% to 82% for SFH-Mg/Al-LDHs, 12% to 86% for SFH-Mg/Al-LDHs at 300 °C, 17% to 97% for SFH-Mg/Al-LDHs at 350 °C, and 11% to 91% for SFH-Mg/Al-LDHs at 350 °C, as per Figure 5. The removal efficacy improves due to the increased number of adsorption sites and function groups as well as the increased pore volume and surface area provided by higher adsorbent doses (14, 27). Nonetheless, the removal efficacy of MER was not notably altered beyond the dosage of 1.5 g/50 mL. The overlapping of active sites at elevated dosage levels could be the cause for this phenomenon. Thus, the accumulation of exchanger particles negated an effective increase in surface area (21, 50). Distinct adsorbents divulged equivalent findings in several other antibiotic adsorption processes (14, 28).

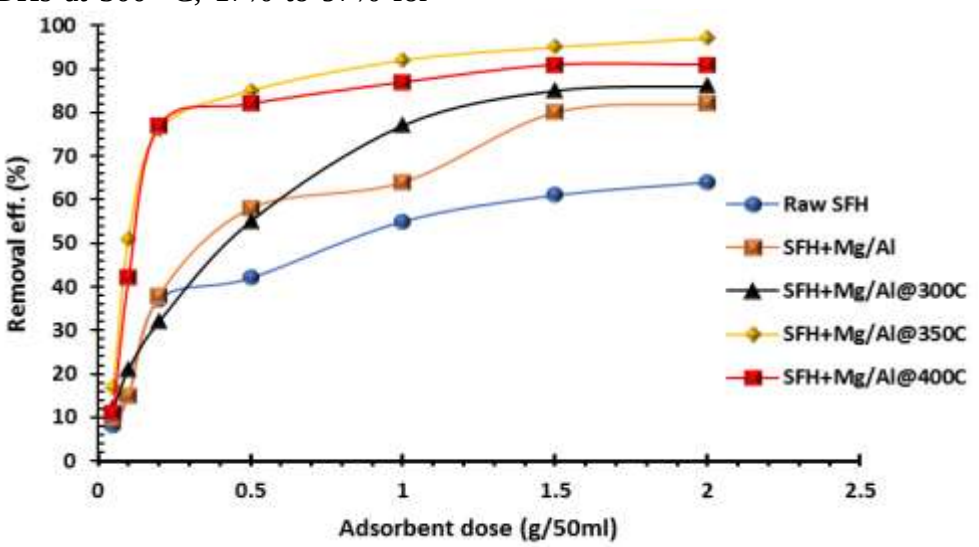

Fig. 5. Impact of adsorbent dose on removal efficacy of MER (temperature = 25°C, agitation speed = 150 rpm, contact time = 4 hour, pH = 6, and C_o = 100 mg L^{-1})

Impact of pH

The surface morphology and chemistry of the adsorbents are substantially impacted by pH which, in turn, impacts the performance of LDH and its hybrids. The ionic chemistry of a solution and the surface charge of the adsorbent explicate the mentioned phenomenon (15). The pH is modified via the incorporation to the solute of base and acid with the objective of investigating the impact of pH on adsorption capacity. The pH of the solution impacts alterations to the ionization state of organic compounds. As seen in Figure 6, a contact time of 240 minutes, adsorbents dosage of 0.5 g/50 mL, and an initial MER concentration of 100 mg/l are used to evaluate the removal efficacy of MER as a function of solution pH between 2 and 9. The removal efficacy diminished when the solution pH superseded 7, while it increases up to said value such as when the solution pH increased from 3 to 7. Within aqueous solutions, the reduced competition of H^+ ions with MER molecules regarding active sites contributes to the enhanced removal efficacy alongside the low protonation of functional groups on the adsorbent surfaces (58). The adsorption starts to diminish when the electrostatic repulsion between the negatively charge adsorbate (MER) and the adsorbent occurs and the positively charged adsorbent turns negative, upon the solution pH superseding a value of 7 (4). The majority of the MER was existent as anionic species when the pH was between 8 and 9 (> pKa 8.31). At the same time, the negative charging of SFH-Mg/Al-LDHs occurs due to the ionizing of OH- and multiple other Lewis acid sites on the SFH-Mg/Al-LDHs. Significant electrostatic repulsion between the negatively charged MER and the surface of the SFH-Mg/Al-LDHs can lead to a diminished adsorption affinity (47).

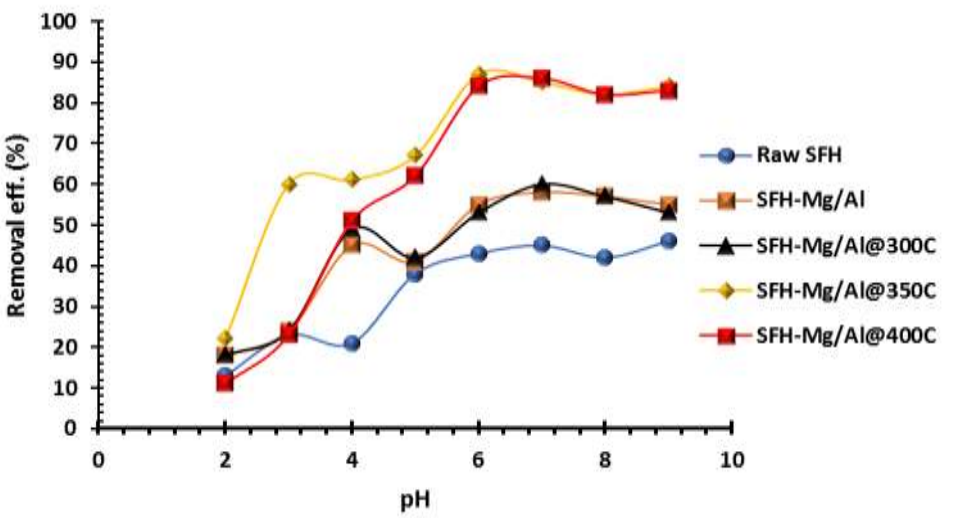

Fig. 6. Impact of pH on removal efficacy of MER (temperature = 25°C, adsorbents dose = 0.5 g/50 mL, contact time = 4 hour, agitation speed = 150 rpm, Co = 100 mg L^{-1})

Impact of initial MER concentration

Within the adsorption process, a substantial supportive factor is the initial concentration of the pollutant, which, in turn, can help surpass the mass transmission resistance of dissolved materials among the aquatic and solid stages (37). As illustrated in Figure 7, a contact time of 240 min, adsorbents dosage of 0.5 g/50 mL, and pH 6 was used to analyze the removal efficacy and how it is impacted by the initial concentration of MER which was between 10 and 350 mg L^{-1}. As the initial concentration rose from 10 to 350 mg L^{-1}, the removal efficacy lessened while low initial concentrations led to high removal efficacy of MER reached to 98%. Larger initial concentrations of MER could need more active site which explicates the drop in efficacy. In lower concentrations, every adsorbent can react with the adsorbate molecules, thereby eliminating them from the solution due to the high ratio of total adsorbate molecules to adsorbent active sites (44). As aforementioned, increases in MER concentration led to the reduced elimination of MER as a result of the saturation of active sites numbering too few to interact with every adsorbent. Nevertheless, a rise in initial concentration elevates the

adsorption capacity when at equilibrium as the resistances to mass transfer of antibiotics between the SFH-Mg/Al-LDHs and the aqueous are surpassed by the increasing concentration gradient (14). The adsorption of several antibiotics by distinct adsorbents has produced equivalent findings, as per the literature (14, 44).

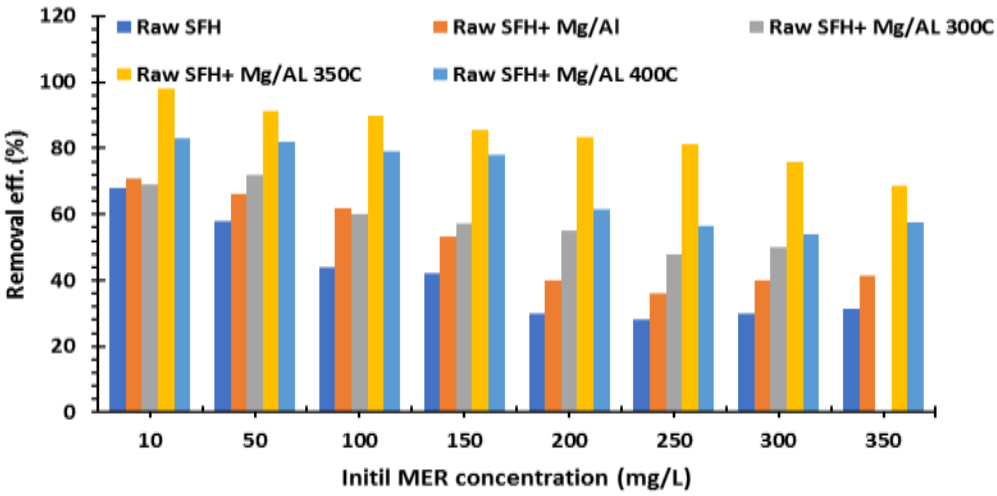

Fig. 7. Impact of initial concentration on removal efficacy of MER (temperature = 25°C, adsorbents dose = 0.5 g/50 mL, contact time = 4 hour, agitation speed = 150 rpm, pH = 6)

Impact of contact time

The effective implementation of adsorbents for practical uses is influenced crucially by the vital parameter of contact time (7). Figure 8 displays an adsorbents dosage of 0.5 g/50 mL, contact time between 3 and 360 minutes, 100 mg/l initial MER concentration, and pH 6 to portray the dependence of removal efficacy of MER on the contact time. The attainment of equilibrium and the use of active sites slowed the rise in the removal efficacy of MER in the second stage which was preceded, in the opening time course of adsorbents process, by an extremely fast removal rate of MER. In the opening 2 hours, the removal percentage experiences a swift increase. The leftover active sites on the adsorbent, the availability of the bare surface area, and the rapid transfer to the surface of prepared adsorbents particles of adsorbate ions via the increased driving force could explicate the rapid adsorption observed in the opening phase (4, 60).

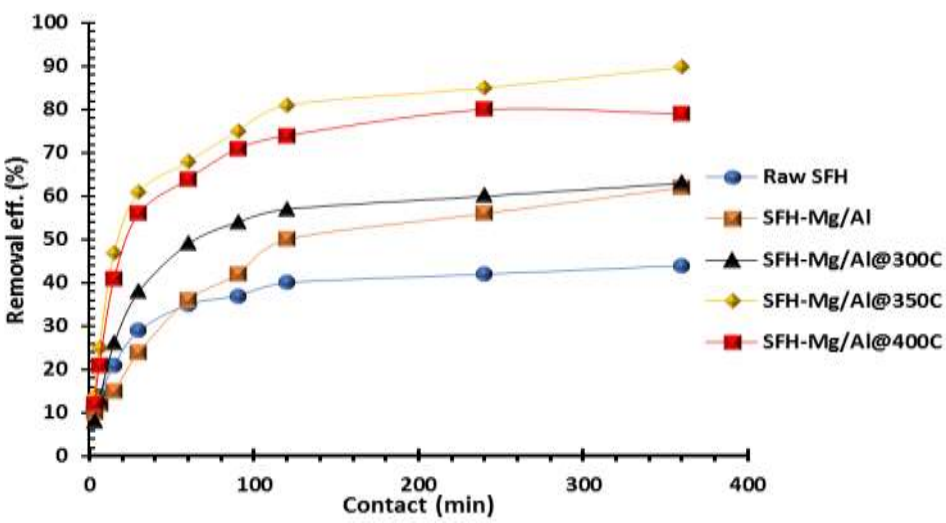

Fig. 8. Impact of contact time on removal efficacy of MER (temperature = 25°C, adsorbents dose = 0.5 g/50 mL, initial concentration = 100 mgL^{-1}, agitation speed = 150 rpm, pH = 6)

Adsorption kinetics

Adsorption efficacy is impacted by a crucial feature known as adsorption kinetics (29). The shaking of the solution for 360, 240, 120, 90, 60, 30, 15, 6, and 3 minutes took place after the amalgamation of 0.5 g of raw SFH-Mg/Al-LDHs at 400 °C, SFH-Mg/Al-LDHs at 350 °C, SFH-Mg/Al-LDHs at 300 °C, SFH-Mg/Al-LDHs, and SFH adsorbent with 50 mL (100 mg L^{-1}) of MER solution in this paper. The

intraparticle diffusion model, the pseudo-first order model, and the pseudo-second order model were used to examine the kinetics data and the mechanism of adsorption while identifying the rate of controlling step (4). The mentioned model's mathematical expressions are presented below:

Equation 3 below outlines the pseudo-first order rate expression of Lagergren (33):

$$\ln(q_e - q_t) = \ln q_e - k_1 t \quad (3)$$

The quantity of meropenem adsorbed ($mg \cdot g^{-1}$) at time t (min) and equilibrium is represented by q_t and q_e respectively. The slope of the linear plots of $\ln(q_e–q_t)$ against t generates the rate k_1 and the first-order rate constant (min^{-1}) is represented by k_1.

The exchange or sharing of electrons between adsorbate and adsorbent in the chemical adsorption process including valence forces could be the rate-limiting step which, in turn, serves as the foundational assumption of the pseudo-second order model (60). The equation stated below can be presented in such a form given that the quantity of actives sites employed on the adsorbent are assumed to be proportional to the adsorption capacity (52):

$$\frac{t}{q_t} = \frac{1}{k_2\, q_e^2} + \frac{1}{q_e} t \quad (4)$$

The pseudo-second order rate constant is represented by k_2 ($g \cdot mg^{-1} \cdot min^{-1}$) and a plot of t/q_t against t was used to determine the values of q_e and k_2. The role of diffusion is often predicted via the implementation of the intra-particle diffusion model (58). Below lies the intraparticle diffusion equation (4):

$$q_t = k_p t^{\frac{1}{2}} + C \quad (5)$$

The intraparticle diffusion rate constant ($mg\ g^{-1}\ min^{-1/2}$) and the intercept ($mg\ g^{-1}$) are represented by k_p and C respectively. Table 3 includes the C factors, k_1, k_2, q_{cal}, k_p, q_e, and other kinetic parameters that in tandem with such models produced the correlation coefficients (R^2). A linear relation with R^2 over 0.999 was demonstrated by the plots in line with the pseudo-second order kinetics assumption, as seen in Table 3. Additionally, fitting findings determined from experimental data were almost equivalent to the meropenem adsorption quantities attained from the same data. Thus, the pseudo-second order kinetics was adhered to within the meropenem adsorption procedure on SFH-Mg/Al-LDHs at 400 °C, SFH-Mg/Al-LDHs at 350 °C, SFH-Mg/Al-LDHs at 300 °C, SFH-Mg/Al-LDHs, and raw SFH adsorbents. The quantity of actives sites on the sorbent is proportional to the adsorption capacity and chemical interactions regulate the adsorption rate, as per the assumption of the pseudo-second order model (22, 52).

Table 3. The coefficients of regression and the kinetic model parameters for meropenem adsorption

Models		Parameters				
Pseudo-first order	**Adsorbents**	**q_{exp} (mg/g)**	**q_{cal} (mg/g)**		**K_1**	**R^2**
	Raw SFH	**4.4**	**2.65**		**0.0097**	**0.9220**
	SFH-Mg/Al-LDHs	**6.2**	**5.56**		**0.0105**	**0.9781**
	SFH-Mg/Al-LDHs at 300°C	**6.3**	**4.21**		**0.0109**	**0.9350**
	SFH-Mg/Al-LDHs at 350°C	**8.98**	**6.51**		**0.0147**	**0.9461**
	SFH-Mg/Al-LDHs at 400°C	**7.9**	**4.49**		**0.0099**	**0.8232**
Pseudo-second order	**Adsorbents**	**q_{exp} (mg/g)**	**q_{cal} (mg/g)**		**K_1**	**R^2**
	Raw SFH	**4.4**	**4.54**		**0.0138**	**0.9991**
	SFH-Mg/Al-LDHs	**6.2**	**6.76**		**0.0035**	**0.9876**
	SFH-Mg/Al-LDHs at 300°C	**6.3**	**6.67**		**0.0066**	**0.9997**
	SFH-Mg/Al-LDHs at 350°C	**8.98**	**9.32**		**0.0059**	**0.9992**
	SFH-Mg/Al-LDHs at 400°C	**7.9**	**8.34**		**0.0074**	**0.9994**
Intra-particle diffusion	**Adsorbents**	**q_{exp} (mg/g)**	**q_{cal} (mg/g)**	**C**	**K_p**	**R^2**
	Raw SFH	**4.4**	**5.02**	**1.43**	**0.1893**	**0.8254**
	SFH-Mg/Al-LDHs	**6.2**	**6.16**	**-0.67**	**0.5089**	**0.9706**
	SFH-Mg/Al-LDHs at 300°C	**6.3**	**7.62**	**1.04**	**0.3469**	**0.8362**
	SFH-Mg/Al-LDHs at 350°C	**8.98**	**10.71**	**1.93**	**0.4627**	**0.8118**
	SFH-Mg/Al-LDHs at 400°C	**7.9**	**9.81**	**1.74**	**0.4255**	**0.7919**

q_{exp} is experimental, q_{cal} is theoretical.

Adsorption isotherm

Further comprehension of the interactions between an adsorbent and an adsorbate is divulged while the adsorption capacity of an adsorbent is assessed through an adsorption isotherm (29). MER removal from aqueous solutions with distinct initial concentrations of

MER – 350, 300, 250, 200, 150, 100, 50, 10 mg L^{-1} – with 240 minutes of contact time, pH 6, 150 rpm agitation speed, and adsorbents dosage of 0.5 g/50 mL and its ties to experimental equilibrium data were assessed via the investigation of adsorption models. The isotherm data of MER adsorption on SFH-Mg/Al-LDHs at 400 °C, SFH-Mg/Al-LDHs at 350 °C, SFH-Mg/Al-LDHs at 300 °C, SFH-Mg/Al-LDHs, and raw SFH adsorbents is examined via the implementation of the widely used Freundlich and Langmuir equations stated below:

The total monolayer coverage on the adsorbent surface and its correspondent approximation of the maximum sorption capacity led to the selection of the Langmuir isotherm model (28). The mentioned equation is stated below:

$$q_e = \frac{q_m\, b_l C_e}{1+b_l C_e} \qquad (6)$$

The convergence between adsorbents and meropenem (L mg^{-1}), the capacity of adsorption at equilibrium (mg g^{-1}), the concentrations of meropenem at equilibrium (mg L^{-1}), and the maximum capacity of adsorption (mg g^{-1}) in relation to the Langmuir equilibrium constant are represented by b_l, q_m, C_e, and q_e respectively. The single-layer adsorption that forms following the equilibrium form of heterogeneous adsorption mechanisms may not be sufficiently explicated by the Langmuir isotherm. The use of the dimensionless differentiation factor (R_L) can be said to be the core feature of the Langmuir equation. As seen in Equation 7 below, the dimensionless constant is represented by R_L (34):

$$R_L = \frac{1}{1+b_l C_O} \qquad (7)$$

The initial meropenem concentration is represented by C_0 (mg L^{-1}). The adsorption process is irreversible, favorable, linear, and unfavorable when the R_L value is 0, between 0 and 1, equal to 1, and over 1 respectively (6). Adsorption on a heterogeneous surface compatible with diverse affinities serves as the basis for the empirical equation of the Freundlich isotherm equation found below (35):

$$q_e = K_f C_e^{1/n} \qquad (8)$$

The constant giving adsorption intensity and capacity are represented by n K_f respectively. A decent adsorption potential is demonstrated when n values lie between 1 and 10 (16). Table 4 describe the R^2 values for SFH-Mg/Al-LDHs at 400 °C, SFH-Mg/Al-LDHs at 350 °C, SFH-Mg/Al-LDHs at 300 °C, SFH-Mg/Al-LDHs, and raw SFH adsorbents as well as the constants of both isotherm equations. The high correlation coefficient values found in the Freundlich model indicate that mentioned model can outline the adsorption isotherm of MER better than Langmuir's model. The heterogeneous and multi-layer active sites of the adsorbent's surface were the location for the reaction of the MER molecules which links to the MER surfaces consisting of distinct adsorption sites. The complex mechanism of MER adsorption onto the surface of the adsorbents was divulged through the mentioned results. A standard Freundlich isotherm was suggested as the 1/n values were well below 1(28).=

Table 4. Isotherm parameters for the adsorption of MER onto adsorbents

Models		Parameters			
Langmuir	**Adsorbents**	**q_{max} (mg g^{-1})**	**b (mg^{-1})**	**R_L**	**R^2**
	Raw SFH	**15**	**0.0069**	**0.52**	**0.8948**
	SFH-Mg/Al-LDHs	**17**	**0.0114**	**0.42**	**0.8845**
	SFH-Mg/Al-LDHs at 300°C	**30**	**0.0062**	**0.54**	**0.9795**
	SFH-Mg/Al-LDHs at 350°C	**30**	**0.0381**	**0.22**	**0.9947**
	SFH-Mg/Al-LDHs at 400°C	**21**	**0.0273**	**0.27**	**0.9270**
Freundlich	**Adsorbents**	**K_f (mg g^{-1})(mg L^{-1})1/*nf***	**n**	**1/n**	**R^2**
	Raw SFH	**0.44**	**1.77**	**0.56**	**0.9270**
	SFH-Mg/Al-LDHs	**0.72**	**1.86**	**0.54**	**0.9104**
	SFH-Mg/Al-LDHs at 300°C	**0.57**	**1.55**	**0.65**	**0.9874**
	SFH-Mg/Al-LDHs at 350°C	**3.43**	**2.31**	**0.43**	**0.9699**
	SFH-Mg/Al-LDHs at 400°C	**1.79**	**2.17**	**0.46**	**0.9290**

CONCLUSION

The separation of MER from aqueous solutions using SFH-Mg/Al-LDHs and raw SFH adsorbent specimens was tested for in this paper. A MER removal percentage of 67% and 51% was achieved by the SFH-Mg/Al-LDHs

and raw SFH respectively, as per the findings of this paper. The removal efficacy of MER was found to be enhanced via the incorporation of Mg/Al-LDHs to SFH. This study also involved the examination of the impact on SFH-Mg/Al-LDHs by calcination temperatures between 300 °C and 400 °C. At a calcination temperature of 350 °C, the SFH-Mg/Al-LDHs demonstrated its maximum removal percentage of MER reaching 91%. The best adsorption conditions were determined by undertaking multiple batch studies. When subjected to the ideal conditions, the removal efficacy of MER reached 98% upon the implementation of the adsorption process. The intraparticle diffusion rate mechanism, the pseudo-first order, and the pseudo-second order served as the basis for the kinetic investigation of MER on adsorbents. The adsorption of MER could be regulated by the chemisorption that functions as the rate limiting step and the pseudo-second order model can outline the adsorption kinetics. The mathematical expressions of the adsorption equilibrium data were presented via the Langmuir and Freundlich adsorption isotherm models. The optimum correlation for the adsorption process was demonstrated by the Freundlich isotherm model. The heterogeneous and multi-layer active sites of the adsorbent's surface were the location where the MER molecules reacted. Overall, the separation of MER from aqueous environments can be carried out via the eco-friendly, efficient, and economic biomass system proposed in this paper.

REFERENCES

1. Abd, I. N. and M. J. Mohammed-Ridha. 2021a. Simultaneous adsorption of tetracycline and amoxicillin by cladophora and spirulina algae biomass. Iraqi J. Agric. Sci. 52: 1290–1303

2. Abd, I. N. and M. J. Mohammed-Ridha. 2021b. Tetracycline antibiotic removal from aqueous solution using cladophora and spirulina algae biomass. Iraqi J. Agric. Sci. 52: 336–347

3. Abdulhussein, S. A. and A. I. Al wared. 2019. Single and Binary Adsorption of Cu(II) and Ni(II) Ions from Aqueous Solutions by Sunflower Seed Husk. Assoc. Arab Univ. J. Eng. Sci. 26: 35–43

4. Ahmed, M. J. and S. K. Theydan. 2014. Fluoroquinolones antibiotics adsorption onto microporous activated carbon from lignocellulosic biomass by microwave pyrolysis. J. Taiwan Inst. Chem. Eng. 45: 219–226. Taiwan Institute of Chemical Engineers

5. Ajmal, M., R. Ali Khan Rao, S. Anwar, J. Ahmad and R. Ahmad. 2003. Adsorption studies on rice husk: Removal and recovery of Cd(II) from wastewater. Bioresour. Technol. 86: 147–149

6. Akar, S. T., A. Gorgulu, Z. Kaynak, B. Anilan and T. Akar. 2009. Biosorption of Reactive Blue 49 dye under batch and continuous mode using a mixed biosorbent of macro-fungus Agaricus bisporus and Thuja orientalis cones. Chem. Eng. J. 148: 26–34

7. Akar, T. and S. Tunali. 2005. Biosorption performance of Botrytis cinerea fungal by-products for removal of Cd(II) and Cu(II) ions from aqueous solutions. Miner. Eng. 18: 1099–1109

8. Al-Hemiri, A. A., K. M. Abed and A. W. Al-Shahwany. 2012. Extraction of Pelletierine from Punica granatum L.by Liquid Membrane Technique and Modelling. Iraqi J. Chem. Pet. Eng. 13: 1–9

9. Alsager, O. A., M. N. Alnajrani, H. A. Abuelizz and I. A. Aldaghmani. 2018. Removal of antibiotics from water and waste milk by ozonation: kinetics, byproducts, and antimicrobial activity. Ecotoxicol. Environ. Saf. 158: 114–122. Elsevier Inc

10. Auer, S. M., R. Wandeler, U. Göbel and A. Baiker. 1997. Heterogeneous coupling of phenylethyne over Cu-Mg-Al mixed oxides: Influence of catalyst composition and calcination temperature on structural and catalytic properties. J. Catal. 169: 1–12

11. Bajpai, S., M. Bajpai and N. Rai. 2012. Sorptive removal of ciprofloxacin hydrochloride from simulated wastewater using sawdust: Kinetic study and effect of pH. Water SA 38: 673–682

12. Basile, F., L. Basini, M. D'Amore, G. Fornasari, A. Guarinoni, D. Matteuzzi, G. Del Piero, F. Trifirò and A. Vaccari. 1998. Ni/Mg/Al anionic clay derived catalysts for the catalytic partial oxidation of methane: Residence time dependence of the reactivity features. J. Catal. 173: 247–256

13. Chen, J., Y. Wang, Y. Qian and T. Huang. 2017. Fe(III)-promoted transformation of B-lactam antibiotics: Hydrolysis vs oxidation. J. Hazard. Mater. 335: 117–124. Elsevier B.V

14. Darweesh, T. M. and M. J. Ahmed. 2017. Batch and fixed bed adsorption of levofloxacin on granular activated carbon from date (Phoenix dactylifera L.) stones by KOH chemical activation. Environ. Toxicol. Pharmacol. 50: 159–166. Elsevier B.V
15. Daud, M., A. Hai, F. Banat, M. B. Wazir, M. Habib, G. Bharath and M. A. Al-Harthi. 2019. A review on the recent advances, challenges and future aspect of layered double hydroxides (LDH)– Containing hybrids as promising adsorbents for dyes removal. J. Mol. Liq. 288: 110989. Elsevier B.V
16. Dizge, N., C. Aydiner, E. Demirbas, M. Kobya and S. Kara. 2008. Adsorption of reactive dyes from aqueous solutions by fly ash: kinetic and equilibrium studies. J. Hazard. Mater. 150: 737–746. Elsevier
17. Elmolla, E. S. and M. Chaudhuri. 2011. The feasibility of using combined TiO2 photocatalysis-SBR process for antibiotic wastewater treatment. Desalination 272: 218–224. Elsevier B.V
18. Elmoubarki, R., F. Z. Mahjoubi, A. Elhalil, H. Tounsadi, M. Abdennouri, M. Sadiq, S. Qourzal, A. Zouhri and N. Barka. 2017. Ni/Fe and Mg/Fe layered double hydroxides and their calcined derivatives: Preparation, characterization and application on textile dyes removal. J. Mater. Res. Technol. 6: 271–283. Brazilian Metallurgical, Materials and Mining Association
19. Gao, Y., Y. Li, L. Zhang, H. Huang, J. Hu, S. M. Shah and X. Su. 2012. Adsorption and removal of tetracycline antibiotics from aqueous solution by graphene oxide. J. Colloid Interface Sci. 368: 540–546. Elsevier Inc
20. Girardi, C., J. Greve, M. Lamshöft, I. Fetzer, A. Miltner, A. Schäffer and M. Kästner. 2011. Biodegradation of ciprofloxacin in water and soil and its effects on the microbial communities. J. Hazard. Mater. 198: 22–30. Elsevier
21. Islam, M. and R. Patel. 2010. Synthesis and physicochemical characterization of Zn/Al chloride layered double hydroxide and evaluation of its nitrate removal efficiency. Desalination 256: 120–128. Elsevier B.V
22. Ji, L., W. Chen, L. Duan and D. Zhu. 2009. Mechanisms for strong adsorption of tetracycline to carbon nanotubes: A comparative study using activated carbon and graphite as adsorbents. Environ. Sci. Technol. 43: 2322–2327. ACS Publications
23. Jin, T., W. Yuan, Y. Xue, H. Wei, C. Zhang and K. Li. 2017. Co-modified MCM-41 as an effective adsorbent for levofloxacin removal from aqueous solution: optimization of process parameters, isotherm, and thermodynamic studies. Environ. Sci. Pollut. Res. 24: 5238–5248. Environmental Science and Pollution Research
24. Khodadadi, M., T. J. Al-Musawi, M. Kamranifar, M. H. Saghi and A. H. Panahi. 2019. A comparative study of using barberry stem powder and ash as adsorbents for adsorption of humic acid. Environ. Sci. Pollut. Res. 26: 26159–26169. Springer
25. Koyuncu, I., O. A. Arikan, M. R. Wiesner and C. Rice. 2008. Removal of hormones and antibiotics by nanofiltration membranes. J. Memb. Sci. 309: 94–101
26. Li, B. and T. Zhang. 2013. Different removal behaviours of multiple trace antibiotics inmunicipal wastewater chlorination. Water Res. 47: 2970–2982. Elsevier Ltd
27. Li, G., D. Zhang, M. Wang, J. Huang and L. Huang. 2013. Preparation of activated carbons from Iris tectorum employing ferric nitrate as dopant for removal of tetracycline from aqueous solutions. Ecotoxicol. Environ. Saf. 98: 273–282. Elsevier
28. Liu, H., W. Ning, P. Cheng, J. Zhang, Y. Wang and C. Zhang. 2013. Evaluation of animal hairs-based activated carbon for sorption of norfloxacin and acetaminophen by comparing with cattail fiber-based activated carbon. J. Anal. Appl. Pyrolysis 101: 156–165. Elsevier B.V
29. Liu, Y., C. Dong, H. Wei, W. Yuan and K. Li. 2015. Adsorption of levofloxacin onto an iron-pillared montmorillonite (clay mineral): Kinetics, equilibrium and mechanism. Appl. Clay Sci. 118: 301–307. Elsevier B.V
30. Luo, Y., L. Xu, M. Rysz, Y. Wang, H. Zhang and P. J. J. Alvarez. 2011. Occurrence and transport of tetracycline, sulfonamide, quinolone, and macrolide antibiotics in the Haihe River Basin, China. Environ. Sci. Technol. 45: 1827–1833. ACS Publications
31. Mohammed -Ridha, M. J., Y. R. Hasan and M. A. Ibrahim. 2021a. Adsorption kinetics and mechanisms for meropenem antibiotic removal in batch mode via rice husk functionalized with

Mg/Fe-layered double hydroxides. Sep. Sci. Technol. 56: 2721–2733. Taylor & Francis
32. Mohammed -Ridha, M. J., S. L. Zeki, S. J. Mohammed, K. M. Abed and H. A. Hasan. 2021b. Heavy Metals Removal from Simulated Wastewater using Horizontal Subsurface Constructed Wetland. J. Ecol. Eng. 22: 243–250. Polish Society of Ecological Engineering (PTIE).
33. Mahmoud, M. E., A. M. El-Ghanam, R. H. A. Mohamed and S. R. Saad. 2020. Enhanced adsorption of Levofloxacin and Ceftriaxone antibiotics from water by assembled composite of nanotitanium oxide/chitosan/nano-bentonite. Mater. Sci. Eng. C 108: 110199. Elsevier B.V
34. Mohammed-Ridha, M. J., A. S. Ahmed and N. N. Raoof. 2017. Investigation of the thermodynamic, kinetic and equilibrium parameters of batch biosorption of Pb (II), Cu (II), and Ni (II) from aqueous phase using low cost biosorbent. Al-Nahrain J. Eng. Sci. 20: 298–310
35. Mohammed-Ridha Muna Y Abdul-Ahad. 2014. Adsorption of Levofloxacine Antibacterial from Contaminated Water by Non-Conventional Low Cost Natural Waste Materials. J. Eng. 20: 88–104
36. Mohammed, A. A., T. J. Al-Musawi, S. L. Kareem, M. Zarrabi and A. M. Al-Ma'abreh. 2020. Simultaneous adsorption of tetracycline, amoxicillin, and ciprofloxacin by pistachio shell powder coated with zinc oxide nanoparticles. Arab. J. Chem. 13: 4629–4643.
37. Mohammed, S. J., M. J. M-Ridha, K. M. Abed and A. A. M. Elgharbawy. 2021. Removal of levofloxacin and ciprofloxacin from aqueous solutions and an economic evaluation using the electrocoagulation process. Int. J. Environ. Anal. Chem. 1–19. Taylor & Francis
38. Mohammed, S. J., M. J. M-Ridha. 2021. Optimization of levofloxacin removal from aqueous solution using electrocoagulation process by response surface methodology. Iraqi J. Agric. Sci. 52: 204–217
39. Namasivayam, C., R. Radhika and S. Suba. 2001. Uptake of dyes by a promising locally available agricultural solid waste: coir pith. Waste Manag. 21: 381–387. Elsevier
40. Nikolaou, A., S. Meric and D. Fatta. 2007. Occurrence patterns of pharmaceuticals in water and wastewater environments. Anal. Bioanal. Chem. 387: 1225–1234
41. Omo-Okoro, P. N., A. P. Daso and J. O. Okonkwo. 2018. A review of the application of agricultural wastes as precursor materials for the adsorption of per- and polyfluoroalkyl substances: A focus on current approaches and methodologies. Environ. Technol. Innov. 9: 100–114. Elsevier B.V
42. Ong, S. T., P. S. Keng, S. L. Lee, M. H. Leong and Y. T. Hung. 2010. Equilibrium studies for the removal of basic dye by sunflower seed husk (Helianthus annuus). Int. J. Phys. Sci. 5: 1270–1276
43. Palmisano, R. and L. Campanella. 2015. Photo-Degradation of Amoxicillin, Streptomycin, Erythromycin and Ciprofloxacin by UV and UV/TiO2 Processes. Evaluation of Toxicity Changes Using a Respirometric Biosensor. J. Environ. Anal. Chem. 02
44. Pouretedal, H. R. and N. Sadegh. 2014. Effective removal of Amoxicillin, Cephalexin, Tetracycline and Penicillin G from aqueous solutions using activated carbon nanoparticles prepared from vine wood. J. Water Process Eng. 1: 64–73. Elsevier Ltd
45. Rahmani, A. R., D. Nematollahi, M. R. Samarghandi, M. T. Samadi and G. Azarian. 2018. A combined advanced oxidation process: Electrooxidation-ozonation for antibiotic ciprofloxacin removal from aqueous solution. J. Electroanal. Chem. 808: 82–89. Elsevier
46. Saleh, M. E., A. A. El-Refaey and A. H. Mahmoud. 2016. Effectiveness of Sunflower Seed Husk Biochar for Removing Copper Ions from Wastewater: A Comparative Study. Soil Water Res. 11: 53–63
47. Shaban, M. A. A., M. A. Ibrahim, M. J. M-Ridha and H. A. Hussein. 2020a. Adsorption of meropenem antibiotics from aqueous solutions on multi-walled carbon nanotube. Int. Rev. Civ. Eng. 11: 283–293
48. Shankaraiah, G., S. Poodari, D. Bhagawan, V. Himabindu and S. Vidyavathi. 2016. Degradation of antibiotic norfloxacin in aqueous solution using advanced oxidation processes (AOPs)—A comparative study. Desalin. Water Treat. 57: 27804–27815
49. Soldatkina, L. M., E. V. Sagaidak and V. V. Menchuk. 2009. Adsorption of cationic dyes from aqueous solutions on sunflower husk. J. Water Chem. Technol. 31: 238–243
50. Tahir, H. 2005. Comparative trace metal contents in sediments and liquid wastes from tanneries and the removal of chromium using

Zeolite-5A. Electron. J. Environ. Agric. Food Chem. 4: 1021–1032

51.Tan, X., S. Liu, Y. Liu, Y. Gu, G. Zeng, X. Cai, Z. L. Yan, C. Yang, X. Hu and B. Chen. 2016. One-pot synthesis of carbon supported calcined-Mg/Al layered double hydroxides for antibiotic removal by slow pyrolysis of biomass waste. Sci. Rep. 6: 1–12. Nature Publishing Group

52. Tang, Y., H. Guo, L. Xiao, S. Yu, N. Gao and Y. Wang. 2013. Synthesis of reduced graphene oxide/magnetite composites and investigation of their adsorption performance of fluoroquinolone antibiotics. Colloids Surfaces A Physicochem. Eng. Asp. 424: 74–80. Elsevier B.V

53. Uzun, I. 2006. Kinetics of the adsorption of reactive dyes by chitosan. Dye. Pigment. 70: 76–83. Elsevier

54. Vaccari, A. 1998. Preparation and catalytic properties of cationic and anionic clays. Catal. Today 41: 53–71

55. Wang, J., B. Gao, M. Dou, X. Huang and Z. Ma. 2020. A porous g-C3N4 nanosheets containing nitrogen defects for enhanced photocatalytic removal meropenem: Mechanism, degradation pathway and DFT calculation. Environ. Res. 184: 109339. Elsevier Inc

56. Xiao, Y., H. Chang, A. Jia and J. Hu. 2008. Trace analysis of quinolone and fluoroquinolone antibiotics from wastewaters by liquid chromatography–electrospray tandem mass spectrometry. J. Chromatogr. A 1214: 100–108

57. Xue, L., B. Gao, Y. Wan, J. Fang, S. Wang, Y. Li, R. Muñoz-Carpena and L. Yang. 2016. High efficiency and selectivity of MgFe-LDH modified wheat-straw biochar in the removal of nitrate from aqueous solutions. J. Taiwan Inst. Chem. Eng. 63: 312–317. Elsevier B.V

58. Yi, S., B. Gao, Y. Sun, J. Wu, X. Shi, B. Wu and X. Hu. 2016. Removal of levofloxacin from aqueous solution using rice-husk and wood-chip biochars. Chemosphere 150: 694–701. Elsevier Ltd

59. Yun, S. K. and T. J. Pinnavaia. 1995. Water Content and Particle Texture of Synthetic Hydrotalcite-like Layered Double Hydroxides. Chem. Mater. 7: 348–354

60. Zhang, C. L., G. L. Qiao, F. Zhao and Y. Wang. 2011. Thermodynamic and kinetic parameters of ciprofloxacin adsorption onto modified coal fly ash from aqueous solution. J. Mol. Liq. 163: 53–56. Elsevier B.V

61. Zhao, P., F. Yu, R. Wang, Y. Ma and Y. Wu. 2018. Sodium alginate/graphene oxide hydrogel beads as permeable reactive barrier material for the remediation of ciprofloxacin-contaminated groundwater. Chemosphere 200: 612–620. Elsevier Ltd.